FMRI decoding using sparse neuronal networks

by

Laura Bernabé Miguel

B.A., Escola Politècnica Superior de Castelldefels - UPC, 2005

M.S., Escola Tècnica Superior d'Enginyeria de Telecomunicacions de Barcelona - UPC , 2010

A thesis submitted to the

Faculty of the Graduate School of the

University of Colorado in partial fulfillment

of the requirements for the degree of

Master of Science Thesis

Department of Electrical, Computer, and Energy Engineering

2012

This thesis entitled:
FMRI decoding using sparse neuronal networks
written by Laura Bernabé Miguel
has been approved for the Department of Electrical, Computer, and Energy Engineering

_____

Prof. François G. Meyer

_____

Prof. Shannon Hughes

_____

Prof. Tor Wager

Date _____

The final copy of this thesis has been examined by the signatories, and we find that both the content and the form meet acceptable presentation standards of scholarly work in the above mentioned discipline.

Bernabé Miguel, Laura (Digital Signal Processing)

FMRI decoding using sparse neuronal networks

Thesis directed by Associate Prof. François G. Meyer

In this thesis we propose the use of Sparse Principal Component Analysis to recover neuronal areas in Brain Imaging. We work with functional magnetic resonance imaging data focusing our attention on the dimensionality reduction stage to represent the neuronal activation within the components that contain the maximum temporal variance, tightly related with the hemodynamic response of the neurons. The motivation for the sparse representation follows the idea of the massive modularity definition of the mind where "different neural circuits are specialized for solving adaptive problems".

The results show that the new sparse low dimensional basis (*Eigenbrains*) generated through novel unsupervised algorithms, such as *Augmented Sparse Principal Component Analysis*, perform competitively in terms of neuronal activity prediction. We push the limits of the brain understanding by describing a neuronal network through each *Eigenbrain* component and defining a prediction neuronal model using a linear combination of them.

Dedication

To my great family and all my new and old friends.

Acknowledgements

I want to thank the effort and time of all the members that served in the committee for the defense of this Master's Thesis: Professor Shannon Hughes, Professor Tor Wager and Professor François G. Meyer. I am particularly grateful to my advisor François G. Meyer for working next to me in the development of my research for the last two years.

I really appreciate the important academic contribution of the BBC fellowship program created with the effort of Pete J. Balsells Fundation, Dean Robert Davis and the Generalitat de Catalunya. Education is really basic to continue developing and sharing new knowledge for the whole community and I really believe this is the better way in order to contribute to the growth of Catalonia, specially in this economical difficult period. I am seeking some similar dreams as Mr. Pere Balsells did when he first started his rough path back in the early nineties in USA and I am making the most of this initial support.

Contents

Chapter

Tables

Table

Figures

Figure

Chapter 1

Introduction

1.1 Definition of the problem

Magnetic resonance imaging (MRI) is a powerful medical sensor technique that constructs a structural image of a scanned area of the body. An MRI machine uses powerful magnetic field to align the magnetization of atomic nuclei in the body, and radio frequency fields to systematically alter the alignment of the magnetization. This causes the nuclei to produce a rotating magnetic moment detectable by the scanner. Functional magnetic resonance imaging (fMRI) is a special type of MRI that is used to detect areas of increased brain activity. When a region of the brain becomes active, blood vessels dilate, allowing freshly oxygenated blood to flow quickly to the region. Oxygen-rich blood disturbs the magnetic field of the scanner less than oxygen-depleted blood. This small change is detectable by the scanner and is used to produce the high-dimensional input data set for a mining process stage.

Functional Magnetic Resonance Imaging is a powerful non-invasive medical technique that generates 3D images and quantifies activation of the brain through the blood-oxygen-level-dependency (BOLD). Intensity variations in the fMRI signal related to the neural activity are very small. Also, they are often overlapped with noise from physiological processes, motion effects or hardware scanner distortions.

Each fMRI sample is represented with some hundred thousands of volume units (voxels) which implies over 120 millions for the whole experiment. Hence, typical brain activity interpretation problems deal with noisy, high-dimensional input datasets.

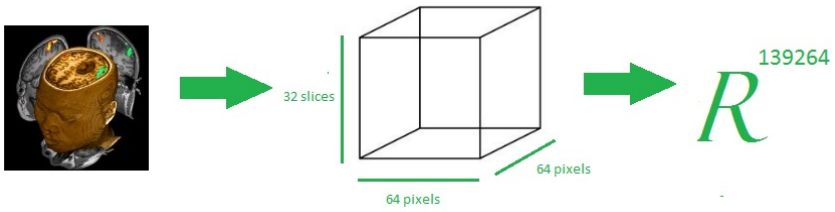

Figure 1.1: 3D High-dimensional fMRI data.

At the beginning of 20^{th} century, the analysis of fMRI data has been reduced to model the relationship between a simple isolated cognitive stimulus and the 3D image. The main purpose was to identify activated brain regions for a simple and independent task, so the brain was stimulated with a well-known input to isolate the neurological processes. The previous experiments combined with some other brain analysis sensors, such as EEG, ECoG, MEG and PET, helped neuroscience to define masks based on lobar anatomy, cortical and subcortical anatomy, and Brodmann areas.

It is widely known in neuroscience that the cytoarchitectural organization of the human cortex is split into several areas, defined by the German anatomist Korbinian Brodmann. Many of the areas Brodmann defined, based solely on their neuronal organization, have been correlated closely to diverse cortical functions. For example, Brodmann areas 1, 2 and 3 are the primary somatosensory cortex; area 4 is the primary motor cortex; area 17 is the primary visual cortex; and areas 41 and 42 correspond closely to primary auditory cortex. However, functional imaging can only identify the approximate localization of brain activations in terms of Brodmann areas since their actual boundaries in any individual brain requires its histological examination.

Within the last half decade, a new fMRI data analysis challenge has been proposed. The goal is to decode complex neurological functions from natural external stimuli, inferring the relevant voxels for any perceptual, behavioral or emotional input applied to the subject under experimentation. The input mimics a natural environment through software video games, movies, etc. Our research wants to explore to what extent the combination of predictive and interpretable modeling of the neuronal activity can provide new insights into functional brain imaging.

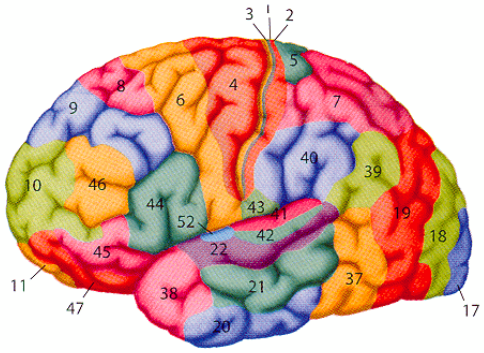

Figure 1.2: Brodmann areas.

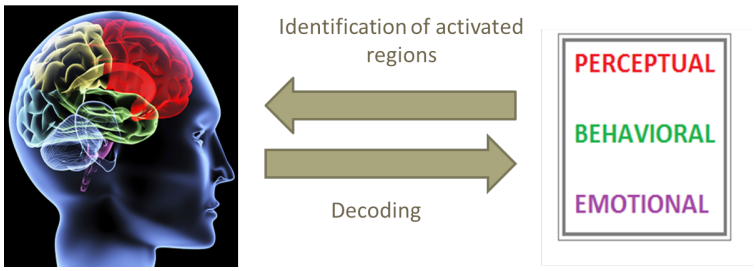

Figure 1.3: fMRI experiment scheme.

Based on the small-world property of clustered local connectivity of the brain networks [3], our strategy assumes that the low-dimensional basis are well-defined by sparse vectors that are correlated with brain functional modules.

1.2 Pittsburgh Brain Activity Interpretation Competition

The fMRI input data for this study is obtained from the Pittsburgh Brain Activity Interpretation Competition 2006 (PBAIC) as a combination of audio and visual stimulus from recorded videos. The data include the rated set of 30 subjective and objective features that parametrize the brain behavior [4].

The PBAIC was an open competition that involved the analysis of fMRI data of individuals watching three approximately 20-minute segments of movies. It included extensive behavioral ratings of experience coding categories (i.e. human faces, tools, arousal, etc.) and multiple finer

levels (i.e. individual actors, happy or sad emotion, etc.). Conceptually, the challenge was to interpret brain activity sufficiently to be able to predict what an observer was experiencing by looking at fMRI data of their brain. The observer's experience was quantified in 13 feature ratings, 3 actor presence ratings and 3 location ratings. Accordingly, high quality 3T EPI fMRI data from three subjects viewing three movie clips were provided. For the first two movie clips, 20 minutes of continuous fMRI data and behavioral feature ratings was provided. For the third clip, only functional data was provided. The original goal was to predict the behavioral rating data of each subject. Accuracy of predictions was determined by correlating predicted behavioral ratings with the empirical ratings for each volume acquisition of the fMRI data (1.75s intervals).

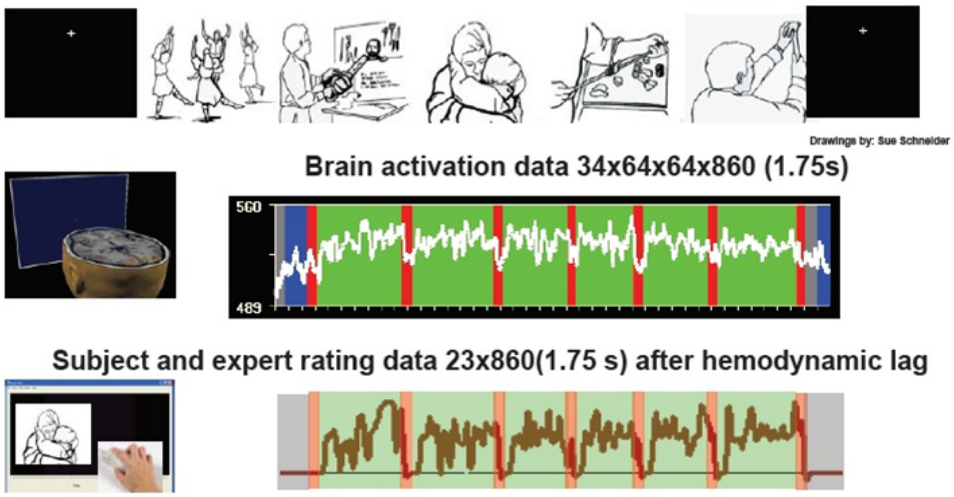

Figure 1.4: Overview of the PBAIC data.

1.2.1 Functional Brain Image Data

Brain image data was collected from three subjects, all of them being native American English speakers.

- Subject 1: male, age 23, right-handed
- Subject 2: female, age 21, right-handed

- Subject 3: male, age 35, right-handed

The fMRI data for the 3 subjects and the 3 movies were captured with the following acquisition parameters:

Table 1.1: Acquisition parameters

Scanner	Siemmens 3T Allegra
TR/TE	1.75s/25ms
Flip angle	76 degress
Field of view	210 mm
Slice thickness	3.5 mm
Slice gap	0
Number of slices	34
xy voxel size	3.28125 mm
xy image dimension	64×64
orientation	axial
Number of volumes (movie 1)	858 volumes
Number of volumes (movie 2)	868 volumes
Number of volumes (movie 3)	900 volumes
Discarded acquisitions	4 seconds

From the contest, we are given the structural MRI and the functional data. The structural data show the different brain tissue areas and their organization; while the functional data contain the measurement of the blood-oxygen-level-dependency (BOLD) within the activated and non-activated areas.

1.2.1.1 Pre-processed data

The "preprocessed" data set contains the functional and structural data that has been preprocessed with the BrainVoyager analysis software [5]. The data pre-processing attempts to remove some standard artifacts that occur in fMRI experiments which may hinder data analysis. The following pre-processing steps were applied to the functional data:

- *Motion Correction:* This pre-processing option adjusts for small head motion. The first volume of the first movie run was specified as the reference volume to which all others were aligned in space by rigid body transformations. The detected head motion of a volume

with respect to the reference volume results in 3 translation and 3 rotation parameters. These detected values are used to translate and rotate the respective volume accordingly to "undo" the detected head motion.

- *Slice Time Correction:* The slices comprising one functional volume are scanned at different moments in time. For functional analysis, a whole functional volume is treated as one data point, as if all slices were measured at the same time. To make this treatment of the data valid (i.e. for interpreting time the same way across a functional volume), the sequentially scanned slices have to be interpolated in time. This pre-processing step temporally interpolates the slices so that all slices can be treated as if they were acquired at the same time.

- *Linear Trend Removal:* fMRI data measurements are subject to slow, low frequency "drifts" over time, that differ from voxel to voxel. Linear trend removal is accomplished through fitting a line to the time course of each voxel using the least-squares regression method. The obtained oblique line is used to remove the linear trend. Note that the mean is restored, so that the detrended dataset is at the same intensity value as the original data.

1.2.1.2 Spatially Normalized data

The spatially normalized data has been pre-processed as per the details in subsection 1.2.1.1, and subsequently spatially normalized. Spatial normalization is a process used to warp the shape of each subjects brain image into a "standard" brain image space. The purpose is to remove morphological differences between subjects, so that data from different subjects can be directly compared, and so that subject data can be compared to standard brain atlases. Once data has been spatially normalized, the corresponding voxels from subjects' brain image data matrices will roughly correspond to anatomical brain regions.

1.2.2 Rated features

Rated features are divided into three categories: Base features, Actors, and Locations. See Fig. 1.5 and Fig. 1.6

- **Base features:** Amusement, Attention, Arousal, Body Parts, Environmental Sounds, Faces, Food, Language, Laughter, Motion, Music, Sadness, and Tools
- **Actor features:** Other People, Mark, Randy, Brad, Tim, Jill, Al, and Wilson
- **Location features:** Other Settings, Backyard, Garage, Kitchen, LivingRoom/DiningRoom, and ToolTime
- Other quantitative features (sound amplitude, video brightness, and blank periods) are provided.

1.3 State of the art of fMRI decoding

Some of the standard techniques in the fMRI literature has included in the same process the feature prediction and coordinates selections stages [6, 7, 8, 9] and stochastic statistical techniques are applied to the noisy high-dimensional fMRI data. Other approaches, like our approach, proceed in two stages; implementing the dimensionality reduction techniques within the modeling stage [10, 11, 12]. These are called non-embedded approaches. In the dimensionality reduction stage, we could enforce interpretation of the data. See Fig. 1.7

In the literature, there exists linear and non-linear dimensionality reduction techniques: PCA, kernel PCA, Isomap, locally linear embedding (LLE), Laplacian eigenmaps, etc. All of the low-dimensional subsapces form the previous algorithms are difficult to interpret. It is almost impossible to infer useful knowledge from them because they have lost spatial properties (voxels in our case) and they are represented by too many coordinates.

The use of Sparse PCA low-dimension representations allows us to reduce the number of coordinates, imposing sparsity in the *Eigenbrains* that represent the principal components. Some

Feature	Description	0	2	4
Faces	Degree to which you see and look at faces on the screen	no face in scene	face and whole body present in scene - face is not the focus of attention*	close up of whole face, facial expressions
Body Parts	Degree to which you see and look at body parts on the screen	nobody in the scene or **shots of head/shoulders only**	whole body in the scene (e.g., people walking)	focus on one part of the body (e.g., hand shake)
Tools	Degree to which tools are seen and used on the screen	no tools in scene	closer shot of tool, not being used (e.g., tool on table)	tool on screen being used (e.g., someone using a drill)
Foods	Degree to which food is seen or eaten	no food in scene	closer shot of food not being eaten or prepared (e.g., food sitting on counter)	food being eaten with clear view of what's being eaten
Motion	Degree to which you see a person or an object moving in the scene; panning is not considered movement	no movement in the scene	NORMAL movement (e.g., walking, cutting vegetables, etc)	FAST or EXTREME movement (e.g., kids running around the house)
Language	Degree to which you hear or read language	no talking or written text on screen	normal conversation*	focus on what is being said, just talking with no other sounds, legible written text on screen (e.g., signs, text on shirts)
Environmental Sounds	Degree to which you hear sounds other than language, music and laugh track; Tool Time audience applause counts	no sounds in scene (people can be talking, music can be playing, laugh track can be heard)	sound at normal volume but isn't the focus of attention (e.g., Tim talking in the background while Al hammers)	sound overwhelms any other sound (e.g., power tool being used)
Music	Degree to which you hear music in the scene	no music in scene	music at normal volume but not focus of attention	music is the focus of attention, people reacting to the music (e.g., dancing, singing), no talking

Figure 1.5: Rated features from PBAIC data.

functional regions related to Brodmann areas are discovered by the sparse estimators.

1.4 Decoding using sparse representation of brain activity

In this thesis we propose a new method to analyze fMRI data. It is organized in two major steps:(a) the implementation of a cognitive decoding model, which interprets cognitive processes;(b) the development of a brain behavioral predictive model, which evaluates the performance through the rated features.

Feature	Description	0	2	4
Laugh Track	Degree to which you hear the laugh track	no laugh track in scene	laugh track does not overwhelm other sounds in the scene, scene doesn't wait for laugh track to end	can only hear laugh track, actors may pause for laugh track
Attention	How attentive and engaged are you to the movie and what is going on in the scene	not paying to attention to video, distracted, "spacing out"	moderately attention to scene - taking in the information	exclusive focus of attention, not thinking about anything else other than the scene
Sadness	How sad is the content of the scene	not sad	moderately sad (e.g., Al having problems with girlfriend)	very sad (e.g., death or discussing death), crying
Amusement	How amusing is the content of the movie	not amusing	moderately amusing (e.g., makes you smile)	very amusing (e.g., makes you laugh out loud)
Arousal	How much does it affect how calm you are (positive or negative)	0 - Exceedingly calm. Low physiological arousal. Not affected by the scene.	2 - Level of arousal/calmness when you are usually watching a sitcom (ie, Home Improvement)	4- Much less calm than in an average sitcom watching session. (e.g., very engaged, heart beating faster, hair on arms standing up, sweating)
* What you would consider to be normal or average as show in the sample clips				

Figure 1.6: Rated features from PBAIC data.

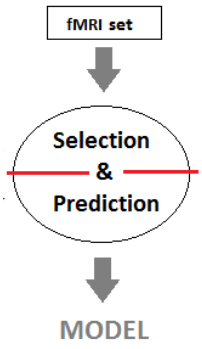

Figure 1.7: Block diagram for fMRI brain decoding

The backbone for the decoding brain activation stage is the detection of significant brain activity through the maximum temporal variation within the voxels in the brain. The previous context fits in the classical principal component analysis (PCA) dimensionality reduction method; nevertheless, it is a poor subspace estimator for our experiments because we focus on high dimensional observations.

We introduce some notations. Let n be the number of time samples or the number of scans; and p the number of voxels in each scan. Let $x(t) \in \mathbb{R}^p$ be a 3D scan collected at a time t, that is reshaped as a row vector.

$$x(t) = \begin{bmatrix} x_1(t) \cdots x_p(t) \end{bmatrix}.$$

Overall, the entire fMRI dataset can be described as a matrix;

$$X = \begin{bmatrix} x_1(1) & \cdots & x_p(1) \\ \vdots & \vdots & \vdots \\ x_1(n) & \cdots & x_p(n) \end{bmatrix}.$$

The number of time samples ($n \approx 850$) is significantly smaller than the number of voxels ($p = 64 \times 64 \times 34$), so the spatial covariance matrix of the input data is not a good estimator of the time variances trends.

In addition, we know that X contains spatially localized significant variables, which means that the principal modes of variation should be localized as well. Also motivated by the concept of Massive Brain Modularity(MMH) - which says that the cognitive brain is conformed by sparse neuronal modules which interact adaptively in order to develop a specific task [13] - we use novel Sparse Principal Component Analysis(SPCA) techniques to decode the brain into meaningful sparse neuronal modules, that we called *Eigenbrains* ($\boldsymbol{e_j}$).

According to the MMH, the mind consists of a multitude of domain-specific *modules* or *mental organs*, each of them with a specialized design that makes it an expert in one area of interaction with the world. Being domain specific, each module is activated by, and only by, mental representations of the problem(s) in its area of expertise [14].

The most significant Sparse Principal Components (the first m with higher variance) are carefully interpreted as active neuronal modules. They sketch some interesting Brodmann areas whose functions are related to the interaction with a movie: primary and auditory association cortex; primary, secondary and associative visual cortex (*V1*, *V2*, *V3*); prefrontal cortex and frontal eye fields, etc.

We organize the sparse principal components in the columns of the E_{brain} rotation matrix $\in \mathbb{R}^{p\times m}$, creating the low-dimensional quasi orthogonal basis. The high-dimensional data is projected onto E_{brain} to create X^{nb};

$$X^{nb} = X \cdot E \tag{1.1}$$

.

And X^{nb}, the low-dimensional data, is defined as follows;

$$X^{nb} = \begin{bmatrix} x_1^{nb}(1) & \cdots & x_m^{nb}(1) \\ \vdots & \vdots & \vdots \\ x_1^{nb}(n) & \cdots & x_m^{nb}(n) \end{bmatrix}$$

.

Such functional networks described by the neurological subspace (E_{brain}) are allowed to be different for each feature, hence, different sets of relevant voxels are selected. The structural design for each network is controlled by the *scattering* (λ_1 and λ_2) and the *sparsity* (λ_3)parameters.

Therefore, an optimal sparse neuronal set of *Eigenbrains* exist for each feature (f). We linearly combine them in order to implement the supervised ridge regression prediction model;

$$f(t) = x_1^{nb}(t)\beta_1 + \ldots + x_m^{nb}(t)\beta_m \tag{1.2}$$

for $t = 1, \ldots, n$. The previous expression shows how much activity is represented through each *Eigenbrain*;and how the domain-specific modules of knowledge and psychological structures are correlated with the output rated features.

Chapter 2

Sparse Principal Component Analysis

In many contemporary datasets, such as in the case of our fMRI study, if we organize the p-dimensional observations to be the rows of an $n \times p$ data matrix X; the number of variables p is often comparable to, or even much larger larger than the sample size n. For example,

- Image recognition: The face recognition problem typically has $p = 1.6 \times 10^6$ observations and the database may contain only a few hundred pictures.
- Shape Analysis: There is a class of methods for analyzing the shape of an object based on repeated measurements that involves annotating the objects for landmarks. The landmarks act as dimensions of the objects.
- Chemometrics: In many chemometric studies the data consists of several thousand spectra measured at several hundred wavelength positions.
- Climate studies: Measurements on atmospheric indicators are taken at a number of monitoring locations over a large temporal extend.
- Functional data Analysis: A speech dataset example consists of 162 observations, each of which is a periodogram of a *phoneme* spoken by a person. Our fMRI experiment focuses on over 850 samples (for each video and subject), and each one of them has $p \approx 10^5$ dimensions.

- Microarray analysis: Gene microarrays present data in the form of expression profiles of several thousand genes for each subject under study.

One of the crucial issues in the analysis of large p datasets is the dimensionality reduction of the feature space[15].

2.1 Review of PCA

Principal component analysis is a variable reduction procedure. This technique is useful when you have obtained data on a number of variables (possibly a large number of variables), and believe that there is some redundancy in those variables. In this case, redundancy means that some of the variables are correlated with one another, possibly because they are measuring the same construct. If there is redundancy, it should be possible to reduce the observed variables into a smaller number of principal components (artificial variables), which account for most of the variance in the observed variables. Technically, a principal component can be defined as a linear combination of optimally-weighted observed variables.

Hence, the central idea of PCA is to reduce the dimensionality of a data set in which there are a large number of interrelated variables, while retaining as much of the variation present in the data set as is possible. This reduction is achieved by transforming into a new set of variables, the principal components, which are uncorrelated, and which are ordered so that the first few retain most of the variation present in the original set of variables.

This unsupervised method starts with n p-dimensional observation vectors, which can be summarized by projecting down onto a m-dimensional subspace. The summary is the projection of the original vectors onto the m directions of the principal components subspace.

$$E_{brain} = \begin{bmatrix} e_1(1) & \cdots & e_m(1) \\ \vdots & \vdots & \vdots \\ e_1(p) & \cdots & e_m(p) \end{bmatrix}$$

There are several equivalent ways of deriving the principal components mathematically. The

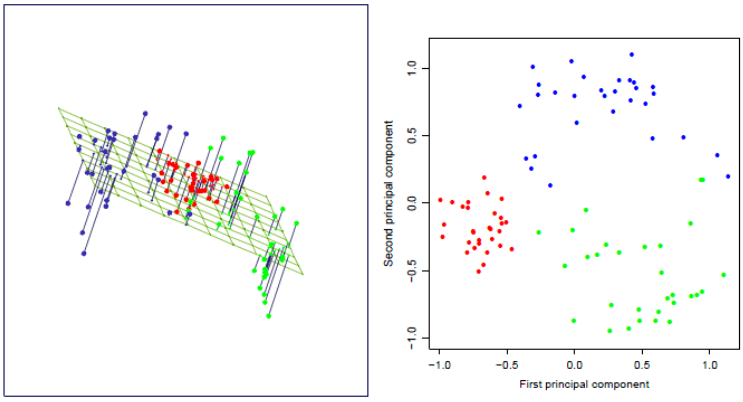

Figure 2.1: Example of PCA projections from [1].

simplest one is by finding the projections which maximize the variance. The first principal component is the direction in feature space along which projections have the largest variance. The second principal component is the direction which maximizes variance among all directions orthogonal to the first. The k_{th} component is the variance-maximizing direction orthogonal to the previous $k-1$ components. There are a total of p principal components.

The goal is to project the p-dimensional feature vectors on to a line through the origin ($e \in \mathbb{R}^p$), so the residual projected error is minimized:

$$min \quad \|x_i - \langle x_i, e\rangle e\|^2 = \quad min \quad \|x_i\|^2 - 2\langle x_i, e\rangle^2 + 1 \tag{2.1}$$

As the first term does not depend on e, it is equivalent to the following expression for all i:

$$max \quad \|x_i\|^2 - 2\langle x_i, e\rangle^2 = \quad max \quad Var\langle x_i, e\rangle \tag{2.2}$$

If we stack all the samples in a matrix X, then the previous optimization problem can be expressed through its covariance matrix Σ_{ij} for all i and j.

$$\Sigma_{ij} = cov(x_i, x_j) = E\left[(x_i - \mu_i)\cdot(x_i - \mu_i)^T\right] \tag{2.3}$$

$$max \quad (e^T \frac{X^T X}{n} e) = \quad max \quad (e^T \Sigma e) \tag{2.4}$$

Finally, by using the *Langrage Multipliers* variables and its derivatives, we infer that the principal components correspond with the eigenvectors of the covariance matrix of the input data. Therefore, computation of the principal components reduces to the solution to an eigenvalue-eigenvector problem for a positive-semidefinite symmetric matrix.

$$\Sigma e = \lambda e \tag{2.5}$$

2.1.1 Properties of PCA

This is a good place to remark that if the data really fall in m-dimensional subspace, created by the first m principal components, then Σ will have only m positive eigenvalues; because, after subtracting off those components, there will be no residuals. The other $p - m$ eigenvectors will all have eigenvalue 0. If the data cluster around a m-dimensional subspace, then $p - m$ of the eigenvalues will be very small.

$$R^2 = \frac{\sum_{i=1}^{m} l_i}{\sum_{j=1}^{p} l_j} \tag{2.6}$$

where l_i and l_j are eigenvalues, and R^2 is the fraction of the original variance of the dependent variable retained by the fitted values. Projections onto the first two or three principal components can be visualized; however, they may not be enough to really give a good summary of the data. Usually, to get an R^2 of 1, you need to use all p principal components.How many principal components you should use depends on the data. In some fields, you can get better than 80% of the variance described with just two or three components.

We have not assumed that the data are drawn at random from some distribution, nor have we assumed that the different rows of the data frame are statistically independent. This is because no such assumption is required for principal components. We simply say these data can be summarized using projections along these directions but nothing about the larger population or stochastic process the data came from.

However, we could add a statistical assumption and see how PCA behaves under those conditions. The simplest one is to suppose that the data are i.i.d draws from a distribution with covariance matrix Σ. Then the sample covariance matrix will converge on Σ_0 as $n \to \infty$. Since the principal components are smooth functions of Σ (eigenvectors), they will tend to converge as n grows. So, along with that additional assumption about the data-generating process, PCA does make a prediction: in the future, the principal components will look like they do now.

The regular principal components are difficult to interpret because they are a linear combination of most of the components in the high-dimensional space. The goal is to represent the fMRI data into some other basis that is more compact and abstract and, indeed, easier to interpret and generate more accurate future predictive models. It is really difficult to infer neurological processes within the 10^5 voxels.

Indeed, as $n << p$ the covariance matrix is a very poor estimator for the temporal trends so we need to seek a sub-covariance matrix within the original $\Sigma \in \mathbb{R}^{n \times p}$. In order to do that, we can use the natural structure of the fMRI that contains spatially localized significant voxels, and try to separate them from the rest of the voxels.

2.2 Sparsity in PCA

In the approach used in *Neuronal Decoding for fMRI images* we focus on measuring brain activation that is related with the temporal variation of all the voxels across time. See Fig. 2.2 We define the $\Sigma^{spatial}$ covariance matrix across the voxels as the original input for the SVD decomposition.

$$\Sigma_{ij} = cov(x_i, x_j) = E\left[(x_i - \mu_i) \cdot (x_i - \mu_i)^T\right] \tag{2.7}$$

where $i, j = 1, \ldots, p$ are all the voxels in our brain.

Therefore, given the covariance matrix in the space domain $\Sigma^{spatial}$, Sparse PCA can be cast as a cardinality-constrained quadratic program, maximizing the variance with a sparse vector $\boldsymbol{e_j}$

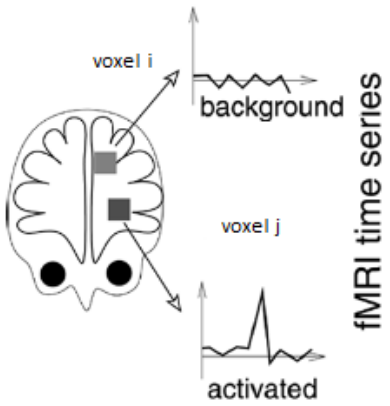

Figure 2.2: fMRI time series for each voxel from [2].

having no more than k non-zero elements.

$$\begin{aligned} max \quad & (e^T \Sigma^{spatial} e) \\ subject \quad & e^T e = 1 \\ & \|e_j\|_0 \leq k \end{aligned} \tag{2.8}$$

This optimization problem is non-convex, NP-hard and therefore intractable [16]. Therefore, it has entailed the development of novel mathematic algorithms in the unsupervised dimensionality reduction literature within the half decade such as: Iterative thresholding sparse PCA (ITSPCA) by Ma (2011) [17], Augmented sparse PCA (ASPCA) by Paul and Johnstone (2007) [15], Correlation augmented sparse PCA (CORSPCA) by Nadler (2009)[18], Sparse PCA via regularized SVD (sPCA-rSVD) by Shen and Huang(2008)[19], Generalized Power Method for Sparse Principal Component Analysis by Jorne,Nesterov,Richtrik and Sepulchre (2010) [20] , etc.

Different thresholding techniques are used to reduce the number of dimensions from the regular principal components; but they do not ensure complete orthogonality among the components within the low-dimensional subspace, although we will see in the following sections that they are pretty close to be uncorrelated.

Augmented Sparse PCA (ASPCA) is considered the best tool for our experiments because we

can make a biological interpretation throughout all the stages of the algorithm. We can understand the low dimension *Eigenbrains* subspace in terms of neurological processes.

Most developments in sparse PCA methodologies typically start with a certain optimization formulation of PCA and then induce a sparse solution by introducing appropriate penalties or constraints. Moreover, when Σ has sparse leading eigenvectors it becomes possible to estimate them consistently under high-dimensional settings.

It is also necessary to estimate the background noise variance for the experiments for all the approaches in order to normalize the data. Assuming normality distributions of the observations we calculate its value as $\widehat{\sigma}^2 = median(Var(x_j))$.

Some of the novel algorithms to estimate the sparse PCA components are reviewed in the following section.

2.2.1 Iterative Thresholding Sparse PCA (ITSPCA)

The ITSPCA paper [17] by Ma focus on finding principal subspaces of $S($ variable used to defined the covariance matrix in the previous paper) spanned by sparse leading eigenvectors, as opposed to finding each sparse vector individually. One of the reasons for this is that individual eigenvectors are not identifiable when some of the leading eigenvalues are identical or close to each other. Also, if we view PCA as a dimension reduction technique, it is the low-dimensional subspace onto which we project data that is of the greatest interest. A new iterative thresholding algorithm is proposed to estimate principal subspaces, which is motivated by the orthogonal iteration method in the matrix computation literature. In addition to the usual steps of orthogonal iteration, an additional thresholding step is added to seek a sparse basis for the subspace.

When the covariance matrix follows the spiked covariance model [21], the algorithm is shown to yield a uniformly consistent subspace estimator.

Algorithm 1: ITSPCA (Iterative thresholding sparse PCA)

Input:

1. Sample covariance matrix S;
2. Target subspace dimension m;
3. Thresholding function η, and threshold levels γ_{nj}, $j = 1, \ldots, m$;
4. Initial orthonormal matrix $\widehat{Q}^{(0)}$.

Output: Subspace estimator $\widehat{\mathcal{P}}_m = \text{ran}(\widehat{Q}^{(\infty)})$, where $\widehat{Q}^{(\infty)}$ denotes the $\widehat{Q}^{(k)}$ matrix at convergence.

repeat

  Multiplication: $T^{(k)} = (t_{\nu j}^{(k)}) = S\widehat{Q}^{(k-1)}$;

  Thresholding: $\widehat{T}^{(k)} = (\widehat{t}_{\nu j}^{(k)})$, with $\widehat{t}_{\nu j}^{(k)} = \eta(t_{\nu j}^{(k)}, \gamma_{nj})$;

  QR factorization: $\widehat{Q}^{(k)}\widehat{R}^{(k)} = \widehat{T}^{(k)}$;

until *convergence*;

(1) Multiplication: $T^{(k)} = AQ^{(k-1)}$;

(2) QR factorization: $Q^{(k)}R^{(k)} = T^{(k)}$.

Figure 2.3: ITSPCA algorithm.

2.2.2 Augmented Sparse PCA (ASPCA)

For the more general multiple component case, Paul and Johnstone [15] proposed an augmented sparse PCA method to estimate each of the leading eigenvectors. They showed that their procedure attains near optimal rate of convergence under a range of high-dimensional sparse settings when the leading eigenvalues are comparable and well separated.

The motivation for this approach considers the SPCA estimation scheme studied by Johnstone and Lu (2004)[22]. Suppose you have calculated the sample variances of all the coordinates;i.e, diagonal terms of Σ (being the covariance matrix) are denoted by $\sigma_1^2, \ldots, \sigma_p^2$. The general pipeline of the method is as follows:

- Define I to be the set of indices $k \in \{1, \ldots, p\}$ such that $\sigma_k^2 > \lambda$
- Let $\Sigma_{I,I}$ be the submatrix of Σ corresponding to the coordinates I. Perform an eigen analysis of $\Sigma_{I,I}$. Denote the eigenvectors by $e_1, \ldots, e_n$ (n = number of observations).

- For $v = 1, \ldots, m$ (m = number of the principal components in the subspace), estimate μ_v by augmenting zeros to all the coordinates that are in $\{1, \ldots, p\}$.

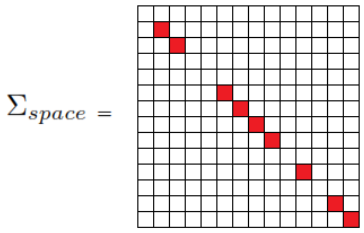

Figure 2.4: Correlation matrix with higher variance voxels selected.

Johnstone and Lu showed that if one chooses an appropriate threshold λ then the estimator is consistent under the sparsity constraint.

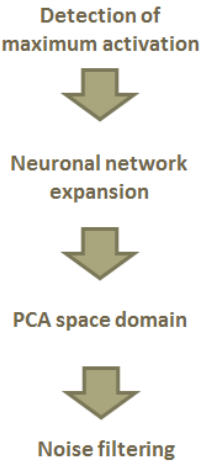

Figure 2.5: Scheme of ASPCA.

The ASPCA aims to address the problem of estimating eigenvectors from a minimax risk analysis viewpoint. Henceforth, the observations are assumed to have a Gaussian distribution. With this condition, the Augmented Sparse Principal Component Analysis (ASPCA) has an optimal rate of convergence over suitable regularity conditions. Moreover, it is also assumed that the leading eigenvalues of the population covariance matrix are distinct, so the eigenvectors are identifiable.

We will go into more details about the ASPCA algorithm and how we adapt it to the *Neurological Decoding* approach in Chapter 3.

2.2.3 Correlation augmented Sparse PCA (CORSPCA)

The CORSCPA analysis in [18] predicted that there would be some gap between the performance of the sparse PCA from Johnstone and Lu (2004) and the possible optimal one. Nadler discussions refers to the work of Bicke and Levina (2008) [23], which assumes that the covariance matrix is sparse, but not necessarily that the eigenvectors are sparse. The key observation is that the assumption of Johnstone and Lu - that individual signals are simultaneously sparse in some unknown basis - implies more than just having relatively few features with large variance. It also implies that these features should be highly correlated among themselves.

Under the assumption of uncorrelated Gaussian noise, this observation suggests an alternate feature selection approach. Rather than working only with the covariance matrix, the structure of the correlation matrix is also analyzed to look for highly correlated variables.

The suggested procedure is as follows:

- Given a data matrix X, compute the covariance (Σ) and correlation matrices(C).
- Estimate the noise variance σ^2.
- Find the sure signal features:
  $I_s = \left\{ i, \frac{\Sigma(i,i)}{\sigma^2} > 1 + \sqrt{\frac{2}{n}} t(\alpha, p) \right\}$
  where
  $t(\alpha, p) = \sqrt{2 \ln p} - \frac{\ln(4\pi \ln p)}{2\sqrt{2 \ln p}} - \frac{\ln \alpha}{\sqrt{2 \ln p}}$
  and α is the confidence level chosen by the user.
- For each $i = 1, \ldots, p$ and $i \notin I_s$ compute
  $E_i = \frac{1}{|I_s|} \sum_{j \in I_s} C(i,j)^2$

- Denote by I_c the set of variables highly correlated to those in I_s:

  $I_c = \left\{ j, j \notin I_s, E_j > \frac{1}{n-1}(1 + \sqrt{2}t(\alpha, p)) \right\}$

Chapter 3

Identificaction of sparse neuronal networks

The pipeline for our approach is described by three major steps:(i) Pre-processing, (ii) Neuronal Decoding and (iii) Prediction of brain activity.

3.1 Pre-processing

In general, fMRI data is really rich and may be grouped into signals of interest and signals not of interest. The **signals of interest** are task-related and function-related. The *task-related* signals are the easiest to model. They are the responses of the brain to a given task. It is conceivable that there are several different types of transiently task-related signals coming from different regions of the brain. The *function-related* signals manifest as similarities between voxels within a particular functional domain. The **signals not of interest** include physiology-related, motion related, and scanner-related signals. Physiology-related signals such as breathing and heart rate tend to come from the brain ventricles (fluid-filled regions of the brain) and areas with large blood vessels present, respectively. Motion-related signals can also be present, and tend to show up as changes across large regions of the image (particularly at the edges of images) [24].

Additionally, changes in the fMRI signal that occur during brain activation are small$(1-5\%)$ and are often contaminated by noise (created by the imaging system hardware or physiological processes), so the cleaner the more sensitive will be the brain activity detection.

In all of our experiments, the input matrix X is created with the pre-processed and spatially normalized fMRI data from the PBAIC contest(See subsections 1.2.1.1 and 1.2.1.2). We do an

additional pre-processing step prior to this approach to clean the data. See Fig. 3.1

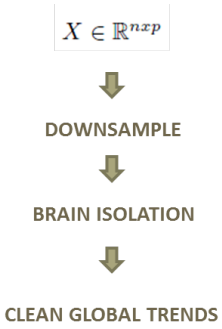

Figure 3.1: Pipeline for the additional pre-prcessing.

Finally, the data is fitted into the assumed input models for the sparse PCA estimators: **independence** between samples and **spiked population model**.

3.1.1 Additional pre-processing

The n fMRI data samples for our experiments are stacked in $X \in \mathbb{R}^{n \times p}$ where each row is filled with the p voxels from a 3D brain image. X is down-sampled and the white-gray matter from all the samples is separated from the outer head area, skull and intra-cranial CSF to build X_{gw}. In this way, high intensity signals from physiological effects are removed from neuronal signals. In order to do that we use standard histogram thresholding techniques with the fMRI signal intensity. See Fig 3.2 and Fig 3.3 .

Finally, we subtract the first and the second principal component of the time covariance matrix $\Sigma^{time} \in R^{n \times n}$ from X_{gw} in order to remove global trend effects - i.e., related to motion artifacts from the head of subject.

$$\Sigma_{ij}^{time} = cov(x_i, x_j) = E\left[(x_i - \mu_i) \cdot (x_j - \mu_j)^T\right]$$
$$X_{gw} = X_{gw} - \langle X_{gw}, pca_{time} \rangle \, pca_{time} \tag{3.1}$$

3.1.2 Fitting the input model

In order to fit the observations into the input data model, they need to be independent and the background noise needs to be white. Each observation is created by the addition of the signal of interest and the signal not of interest;

$$x(t) = u_t e + \sigma z_t, \tag{3.2}$$

where $e \in \mathbb{R}^p$ is the component to be estimated, $u_t \sim N(0,1)$ are i.i.d. Gaussian random effects, σ is the p-vector representation of the background noise level, and $z_t \sim N_p(0, I)$ are independent p-dimensional noise vectors [22].

It is broadly known that fMRI images are related through the hemodynamic response pattern, so, they are not independent.

It has been revealed in some studies that the temporal variation of the BOLD activation is essentially Gaussian [25], so it suffices to uncorrelate each observation to make them independent.

Wavelets have been widely used in various signal and image processing contexts since their mathematical development in the late 1980s, including many prior applications to image compression, non-parametric regression, and problems in brain mapping. However, the single most important property of the discrete wavelet transform is that the correlation between the wavelet coefficients of a signal will generally be small even if the signal itself is highly autocorrelated in time. This is sometimes called the whitening or decorrelating property of the wavelet transform [26]. Hence, by applying 1D wavelet transform to each voxel time sequence values x_j for $j = 1, \ldots, p$ we decorrelate the n observations of the input sets (see Fig 3.5). We recall the definition of the correlation matrix as: $coor(x, y) = \frac{E[(x-\mu_x)(y-\mu_y)]}{\sigma_x \sigma_y}$.

Note that the time scale is no longer in seconds.

The spatial covariance matrix $\Sigma^{spatial}$ must fit in the **spiked population model** to be an optimal input set for ASPCA. This implies that the higher m eigenvalues l_i for $i = 1, \ldots, m$ are above the background noise(σ^2). See Fig 3.6. We apply 3D wavelet transform to potentiate the

intrinsic sparsity of the fMRI images in the new basis. Hence, the entries in $x(t)$ are wavelet coefficients from now on.

As σ^2 is unknown for the fMRI input dataset and assuming normal distributions for the observations, we estimated its value as $\widehat{\sigma}^2 = median(Var(x_j(t)))$

3.2 Neuronal Decoding

The most significant Sparse Principal Components obtained through ASPCA are interpreted as active neuronal modules. They sketch some interesting Brodmann areas, whose functions are related to the audio and visual frames of a movie: primary and auditory association cortex, primary and secondary visual cortex *V1* and d *V2*, associative visual cortex *V3*, prefrontal cortex and frontal eye fields, etc.

We use the first $m = 14$ *Eigenbrains* as the new basis for the low dimensional subspace. As mentioned earlier, the core of the sparse PCA idea focuses on how to choose the appropriate coordinates and all the observations are normalized with the level of background noise σ^2.

Motivated by ASPCA by Paul and Johnstone [15] we apply the algorithm as follows:

(1) Threshold 1: Extract the voxels whith time variance exceeding λ_1 to build($\mathcal{W}(\lambda_1)$). These are the voxels that correspond with neuronal activity. Compute the normalized factor within the coordinates in the previous set. See Fig 3.8

(2) Threshold 2: Compute the normalized correlation between the voxels from $\mathcal{W}(\lambda_1)$ and $\mathcal{W}(\lambda_1)^C$; and select the higher coordinates (exceeding λ_2) to build($\mathcal{W}(\lambda_2)$).See Fig 3.8. It defines the extension of the neuronal network.

(3) Take the union of $\mathcal{W}(\lambda_1) \cup \mathcal{W}(\lambda_2)$. The cardinality of the previous set tunes the cluster properties of the brain modules.

(4) Compute PCA on $(x_k | k \in \mathrm{W}(\lambda_1) \cup \mathrm{W}(\lambda_2))$ and pad them with zeros to extend the coordinates creating $e_i \in R^p$.

(5) Threshold 3: Hard theshold the coordinates in e_i according to the convergence decay factor (λ_3)for regular PCA, in order to filter out the noise .

$$\lambda_3^i = \sqrt{\frac{\lg(b)(1+l_i)}{n \cdot {l_i}^2}} \tag{3.3}$$

$$where \quad i = 1, \ldots, m \quad and \quad b = card(\mathcal{W}(\lambda_1) \cup \mathcal{W}(\lambda_2))$$

(6) Normalize e_i to obtain the eigenbrains.

Finally, we project the high-dimensional input data into E_{brain} creating $X^{nb} \in \mathbb{R}^{n \times m}$ where each row corresponds to an observation in the low-dimensional space ($x^{nb}(t) \in \mathbb{R}^m$).

3.2.1 Scattering and extension of the neuronal network (λ_1 and λ_2)

The *threshold 1* and *threshold 2*, defining the cut-off parameters λ_1 and λ_2, are related to the extension of the original neuronal network that compose the *Eigenbrain*. λ_1 selects the voxels with higher variance related to the brain activation, and λ_2 selects the voxels with smaller variance which are strongly related to the previous activated voxels. The values of the first two thresholds are related because they both scatter the voxels of the network.

To be able to analyze the most significant and interesting combinations of these two thresholds we create a simplified system through labels that represent significant and meaningful values according to the tendency, shown in Fig. 3.7. For *threshold 1* and *threshold 2* we create 10 labels for 20 different values of λ_1 and λ_2 (corresponding to $\gamma_{1,n}$ and $\gamma_{2,n}$ in the original ASPCA algorithm). They have been chosen according with our own simulated experimental results in MATLAB. The higher the values for *threshold 1 - threshold 2*, the more voxels are selected for the sets $\mathcal{W}(\lambda_1)$ and $\mathcal{W}(\lambda_2)$ respectively.

3.2.2 Further Sparsity (λ_3)

The third threshold is used to filter out the noise and shrink the smallest entries for the regular PCA applied over the union of $\mathcal{W}(\lambda_1) \cup \mathcal{W}(\lambda_2)$. The parameter λ_3 tunes the uncorrelation

Table 3.1: Design parameters for maximum prediction score

Threshold 1 - Threshold 2	λ_1	λ_2	card($\mathcal{W}(\lambda_1)$)	card($\mathcal{W}(\lambda_2)$)
1	326.2	47.6	300	90
2	268.7	38.2	400	120
3	233.0	32.4	500	150
4	202.9	25.8	600	180
5	174.3	21.6	700	210
6	150.7	19.0	800	240
7	133.0	16.8	900	270
8	118.2	15.1	1000	300
9	105.9	13.6	1100	330
10	96.4	12.2	1200	360

and the further sparsity of *Eigenbrains* in the new basis. This parameter hard thresholds the entries $i = 1, \ldots, p$ for the different *Eigenbrains* ($e_j(i)$). See Equation 3.4

$$e_i(j) = \begin{cases} e_i(j), & |e_i(j)| > \lambda_3^i, \\ \\ 0, & |e_i(j)| \leq \lambda_3^i, \end{cases} \tag{3.4}$$

$$where \quad i = 1, \ldots, m \quad and \quad j = 1, \ldots, p.$$

The hard thresholding step in *threshold 3* has been organized into 11 labels that are closely related to the final sparsity and correlation of the principal components. The parameter λ_3 which shrinks the smallest values in each *Eigenbrain*(e_j for $j = 1, \ldots, m$) is more agressive the bigger the j index is, so it is not a constant threshold for each label (see Table 3.2 and Fig 3.9). The increase of the (λ_3^j) is related to the convergence decay factor for the regular PCA (see equation 3.3). It corresponds to $\gamma_{3,n}$ in the original ASPCA algorithm.

If λ_3 is small, the *Eigenbrains* are more orthogonal; so, this parameter determines the correlation of the components within the low-dimensional subspace. Fig 3.10

Table 3.2: λ_3 values that correspond with *Threshold 3*

Threshold 3	(λ_3^1)	(λ_3^2)	(λ_3^3)	(λ_3^4)	(λ_3^5)	(λ_3^6)
1	0	0	0	0	0	0
2	0.0088	0.0130	0.0155	0.0159	0.0179	0.0190
3	0.0124	0.0184	0.0219	0.0226	0.0254	0.0269
4	0.0152	0.0225	0.0268	0.0276	0.0311	0.0330
5	0.0176	0.0260	0.0310	0.0319	0.0359	0.0381
6	0.0196	0.0290	0.0346	0.0357	0.0401	0.0426
7	0.0215	0.0318	0.0379	0.0391	0.0440	0.0504
8	0.0232	0.0344	0.0410	0.0422	0.0475	0.0344
9	0.0249	0.0367	0.0438	0.0451	0.0508	0.0467
10	0.0264	0.0390	0.0465	0.0478	0.0538	0.0539
11	0.0278	0.0411	0.0490	0.0504	0.0567	0.0571

3.3 Prediction of brain activity

Possibly the most elementary algorithm that can be kernelized is ridge regression. Ridge Regression is used to find a linear function that models the dependencies between covariates $\{x_i\}$ and response variables $\{f_i\}$, both continuous. The classical way to do this is to minimize the quadratic cost;

$$min\frac{1}{2}\sum_i (f_i - \beta^T x_i)^2. \tag{3.5}$$

To avoid overfit, it is necessary to regularize which can be done by simply penalizing the norm of β. This is sometimes called weight-decay and it is chosen according to a cross validation process.

$$min\frac{1}{2}\sum_i (f_i - \beta^T x_i)^2 + \frac{1}{2}\epsilon \left\|\beta\right\|^2. \tag{3.6}$$

By introducing Lagrange multipliers into the problem the derivation becomes similar to that of the support vector machine problem.

3.3.1 Our predition model

The prediction of a feature $\hat{f}$ at an unknown time t_x is implemented as a supervised learning classifier. We formulate the prediction model using Kernel Ridge Regression;

$$\hat{f}(t_x) = \sum_{i=1}^{n} \widehat{\alpha}_i \cdot \kappa(x^{nb}(t), x^{nb}(tx)), \tag{3.7}$$

where $t = 1, \ldots, n$ represent the training set, $\widehat{\alpha}$ is weighted by the previous set, and κ is a Gaussian kernel.

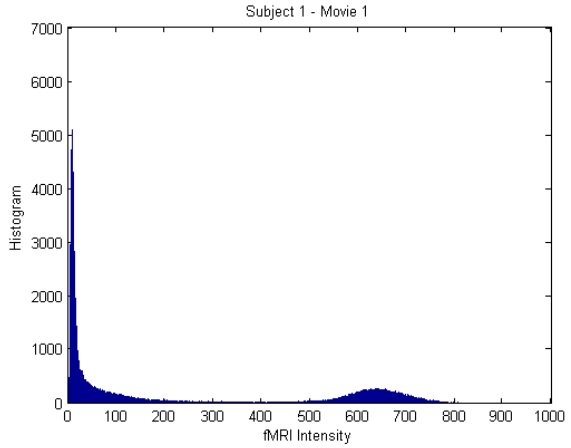

(a)

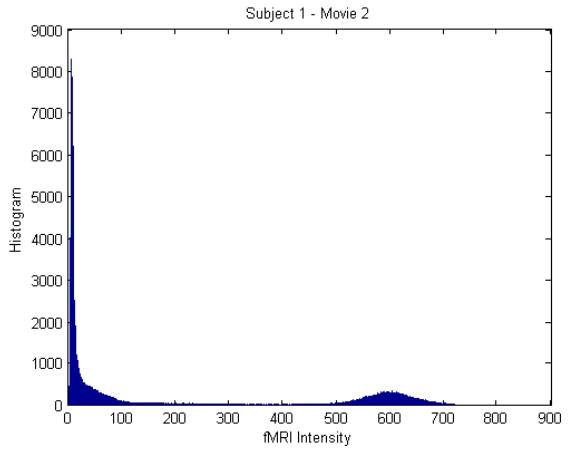

(b)

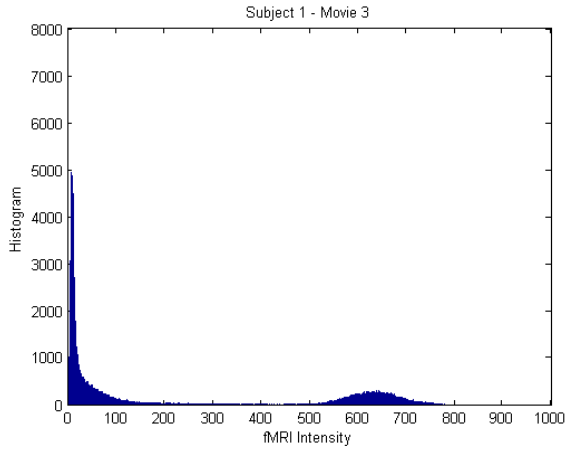

(c)

Figure 3.2: (a)(b)(c) Intensity fMRI histograms for Subject 1 for Movie 1, Movie 2 and Movie 3 respectively.

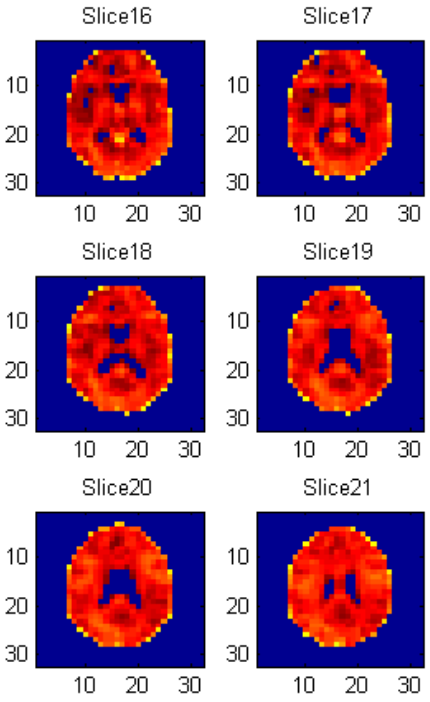

Figure 3.3: White-Gray matter for subject1 Slice 16,17,18,19,20 and 21

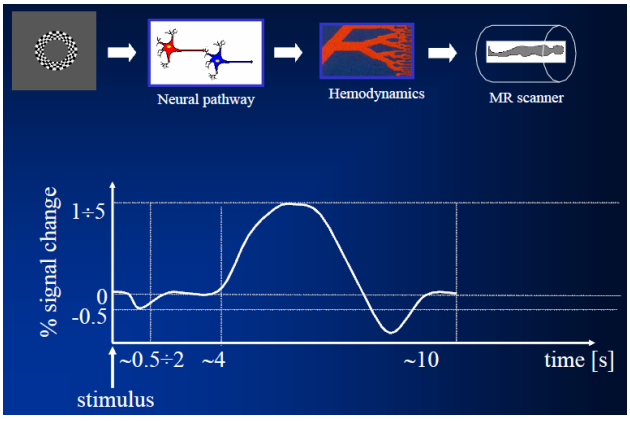

Figure 3.4: Blood Oxygenation Level Dependent contrast fMRI.

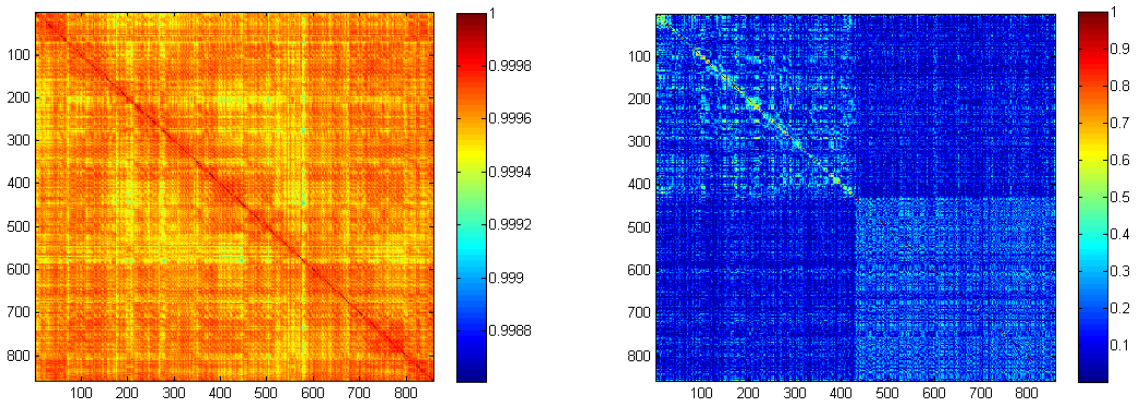

(a) (b)

Figure 3.5: (a) Correlation matrix before 1D wavelet across time (b) Correlation matrix after 1D wavelet across time.

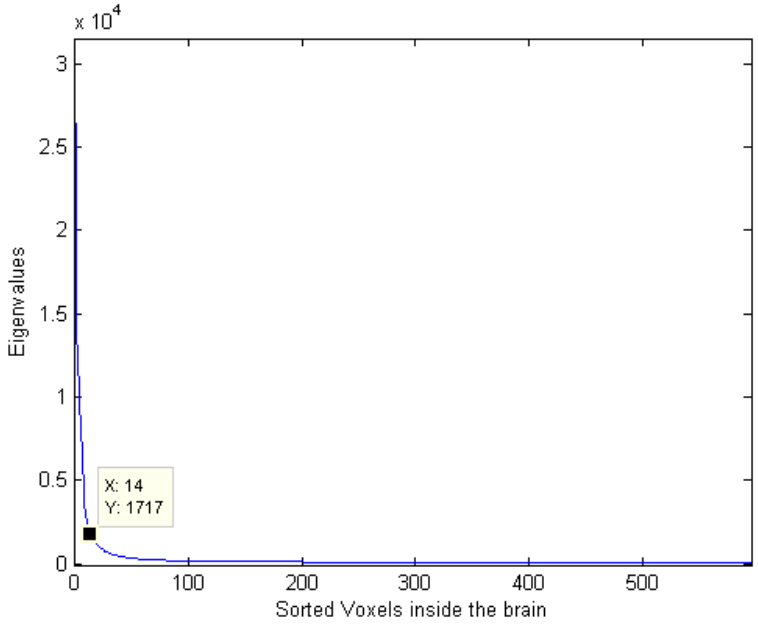

Figure 3.6: Sorted eigenvalues of the covariance matrix. Label in first 14 (m = 14)

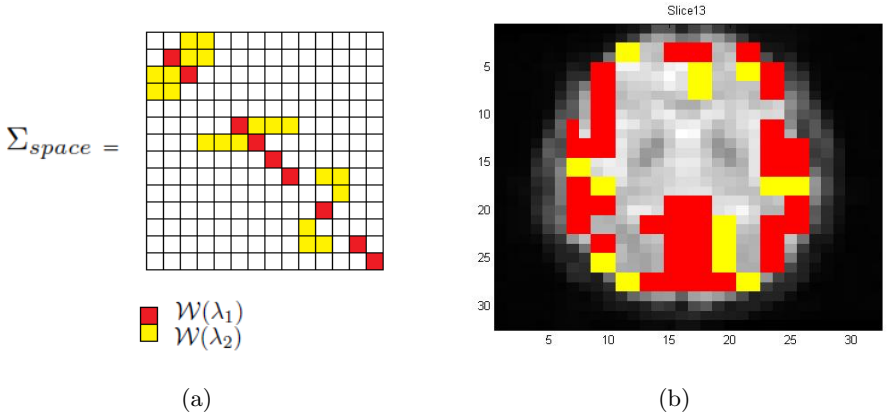

(a) (b)

Figure 3.7: (a) Selection voxels for $\mathcal{W}(\lambda_1)$ and $\mathcal{W}(\lambda_2)$ in $\Sigma^{spatial}$. (b) Selection voxels for $\mathcal{W}(\lambda_1)$ and $\mathcal{W}(\lambda_2)$ in functional magnetic brain image for th_1 and $th_2 = 3$ (500 and 150 voxels respectively).

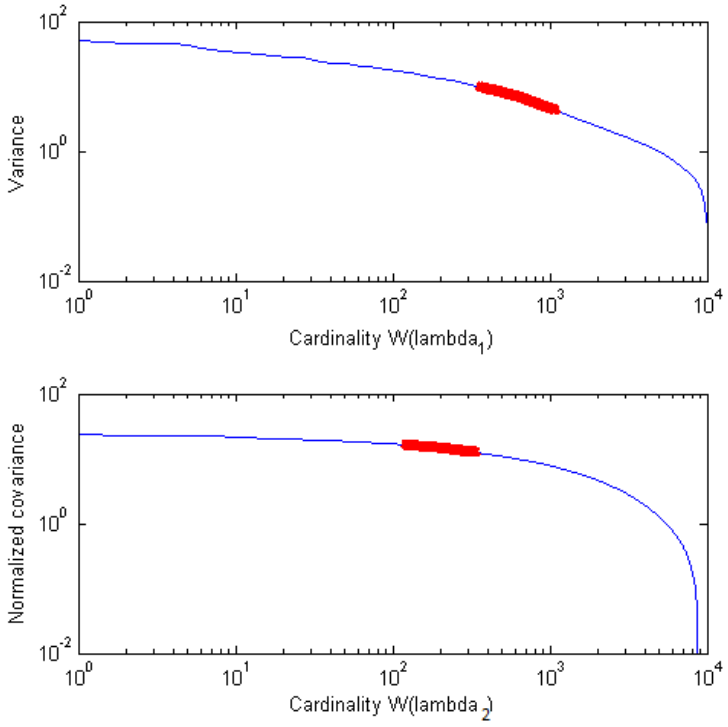

Figure 3.8: (a) Tendency of the Variance for the Threshold 1. In red the range of values evaluated for (λ_1). (b) Tendency of the Variance for the Threshold 2. In red the range of values evaluated for (λ_2).

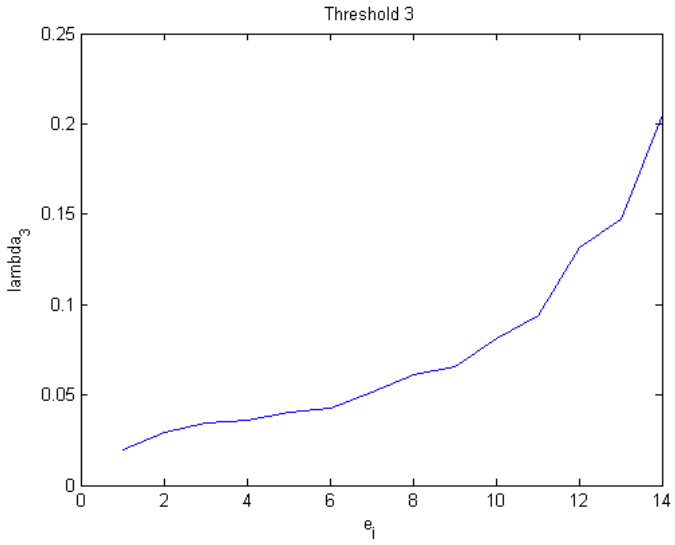

Figure 3.9: Kernel Ridge Regression Prediction score for $m = 14$

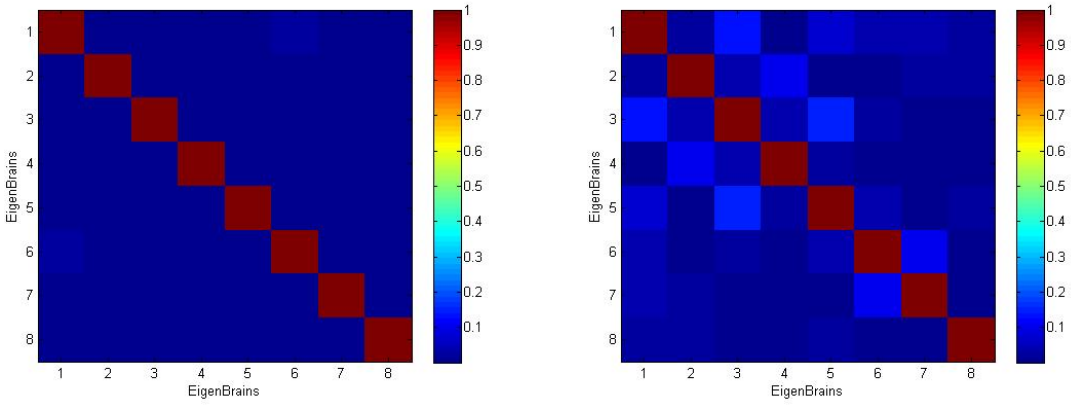

(a) (b)

Figure 3.10: (a) Correlation matrix for $threshold3 = 0$ (b) Correlation matrix for $threshold3 = 3$

Chapter 4

Experiments and discussion

In order to evaluate the performance of the method presented in this paper we measure the normalized correlation between the predicted feature $\hat{f}$ and the expected feature f as follows;

$$score = \frac{\left\langle \hat{f}, f \right\rangle}{\left\| \hat{f} \right\| \cdot \|f\|}. \tag{4.1}$$

The **Sparsity** of the neural network components is measured by adding the L_0 norm of all the *Eigenbrains* within the E_{brain} subspace.

$$Sparsity = \sum_{j=1}^{m} \|e_j\|_0 \tag{4.2}$$

The **Relative Sparsity** is computed to get a sense of how sparse the low-dimensions subspace is in comparison with the total number of voxels p for the whole 3D image ($p = 64 \times 64 \times 34$), so, we define:

$$Relative\ Sparsity = \frac{Sparsity}{m \times p}. \tag{4.3}$$

The 10-fold cross validation is used to weight and evaluate all the prediction scores. It separates the data into ten subsets with $n/10$ observations in each of them. A single subset is retained for testing of the model, and the remaining nine subsets are used as training data.

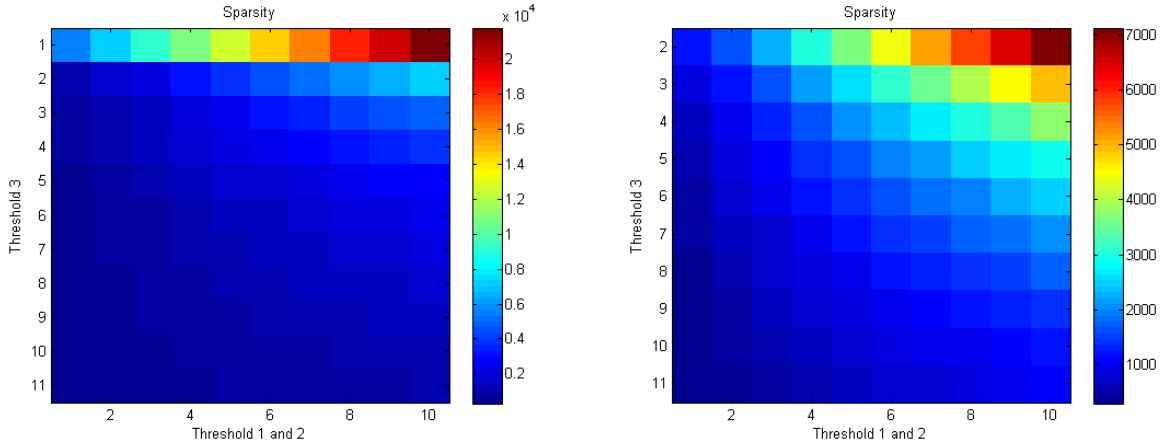

(a) (b)

Figure 4.1: Sparsity as a function of $threshold_1$, $threshold_2$ and $threshold_3$. (a)$threshold_3 = 1, \ldots 11$. (b)$threshold_3 = 2, \ldots 11$.

4.1 Design parameters: score vs. sparsity

Several parameters should be weighted in order to get accurate sparse *Eigenbrains* components at the of the Sparse Augmented Algorithm (ASPCA). The *Decoding Neuronal Network* approach also needs to be tuned by assigning values to the thresholds λ_1, λ_2 and λ_3.

For the studied values within the range for $threshold1$, $threshold2$ and $threshold3$ we achieve the sparsity shown in Fig 4.1 in the E_{brain} subspace composed with 14 *Eigenbrains*. In the graph (b) the y-axes is expanded for ($threshold_3 = 2, \ldots 11$).

In order to fine tune the semi-supervised neuronal decoding approach, we track the feature predictions using 10-fold cross validation of the features with better performance (Body parts - 5, Faces - 7, Language - 9 and Motion - 11) in the prediction model from section 3.3. The optimal design parameters consider a trade-off between the sparsity of e_j and the prediction score.

In Table 4.1 we summarize the values with the maximum prediction score, nonetheless, in Table 4.3 we relax the final score by achieving more sparse and uncorrelated networks.

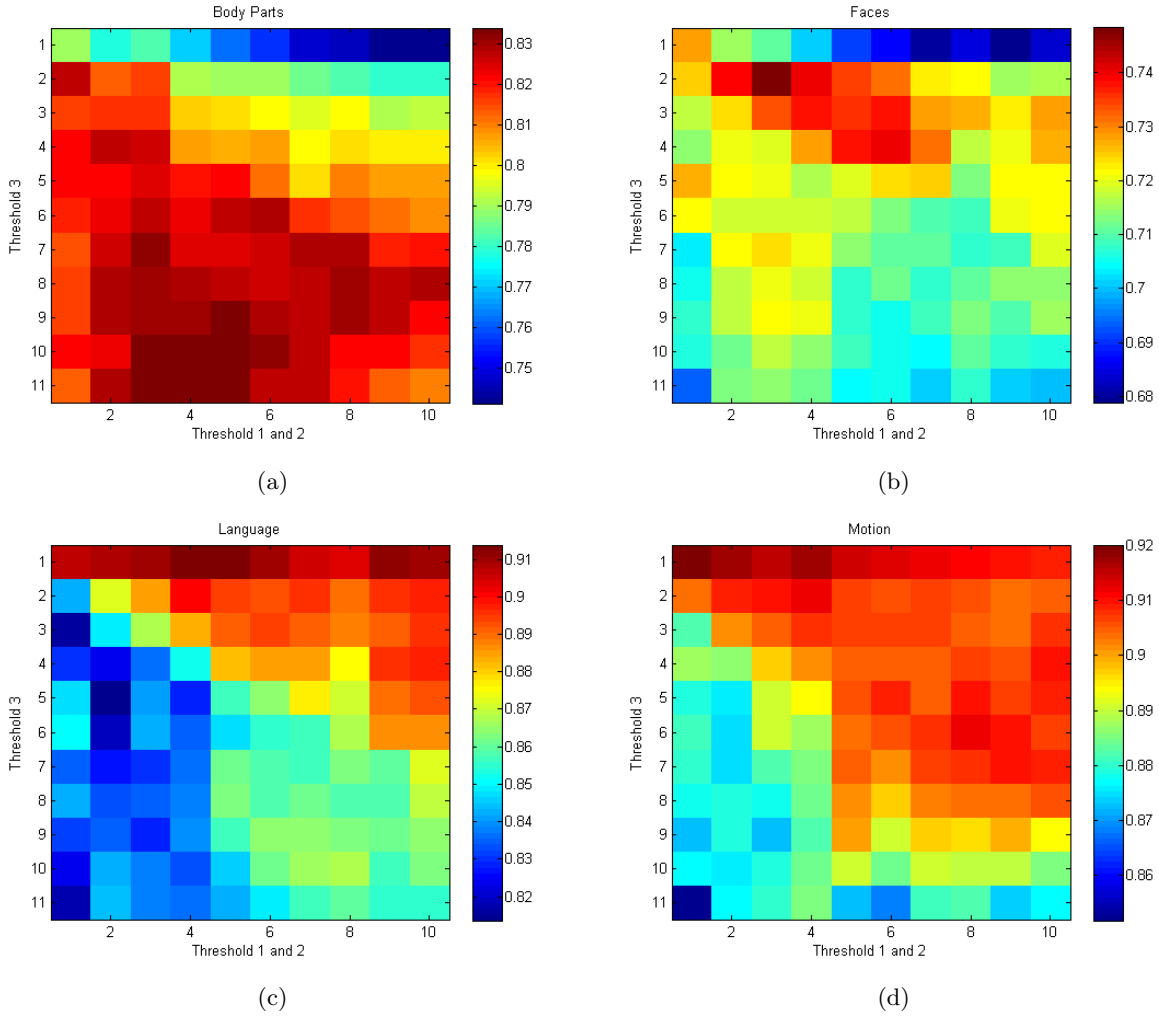

(a) (b) (c) (d)

Figure 4.2: Prediction score as a function of threshold 1(λ_1), threshols 2(λ_2), and threshold 3(λ_3).

Table 4.1: Design parameters for maximum prediction score

Feature	**Prediction score**	**Sparsity**	th_1-th_2	th_3
Body Parts	0.8339	3321	4	10
Faces	0.7483	1181	3	2
Language	0.9138	565	5	1
Motion	0.9201	2328	1	1

4.2 Eigenbrains

Some of the sparse neuronal networks from the optimal values for the feature *Language* are collected in Fig 4.3. These are considered the more interpretable networks, having more aggressive

Table 4.2: Sparsity details for maximum prediction score

Feature	$\|e_1\|_0$	$\|e_2\|_0$	$\|e_3\|_0$	$\|e_4\|_0$	$\|e_5\|_0$	Rel.Sparsity	th_1-th_2	th_3
Body Parts	1184	620	477	418	316	0.72%	4	10
Faces	485	257	213	138	43	0.26%	3	2
Language	338	125	76	26	0	0.12%	5	1
Motion	388	388	388	388	388	0.51%	1	1

Table 4.3: Design parameters for optimal neuronal networks architecture

Feature	**Prediction score**	**Sparsity**	th_1-th_2	th_3
Body Parts	0.8068	2525	5	9
Faces	0.7184	1166	6	4
Language	0.8639	976	9	6
Motion	0.8973	1157	8	6

Table 4.4: Sparsity details for optimal neuronal networks architecture

Feature	$\|e_1\|_0$	$\|e_2\|_0$	$\|e_3\|_0$	$\|e_4\|_0$	$\|e_5\|_0$	Rel.Sparsity	th_1-th_2	th_3
Body Parts	1037	480	353	273	188	0.55%	5	9
Faces	625	234	138	91	41	0.25%	6	4
Language	601	170	68	72	43	0.21%	9	6
Motion	669	205	107	86	55	0.25%	8	6

thresholds, as the prediction score is relaxed.

According to the Brodmann map, the auditory cortex (areas 41 and 42) which processes sound and contributes to our ability to hear, is selected in the *Eigenbrain 2*. The *Eigenbrain 5* activates the areas 17,18,19 in the back of the brain that are associated with the visual cortex (V1,V2 and V3). The frontal eye fields(area 8) and the prefrontal cortex (area 9), involved with eye movements, are shown in *Eigenbrain 4*. See Fig 4.3.

In Fig 4.4, e_2 = yellow,e_3 = pink, e_4 = green and e_5 = red, from the feature *Language* and $threshold_1$ and $threshold_2 = 9$ and $threshold_3 = 6$, are plotted over the same functional magnetic images. It can be inferred that the principal components are largely uncorrelated because they barely overlap. Indeed, they seem to define different functional modules.

In Fig 4.5 and Fig 4.6, the first six optimal architectural neuronal networks, for the feature *Faces* are pictured. The label in this case are: $threshold_1$ and $threshold_2 = 3$ and $threshold_3 = 2$.

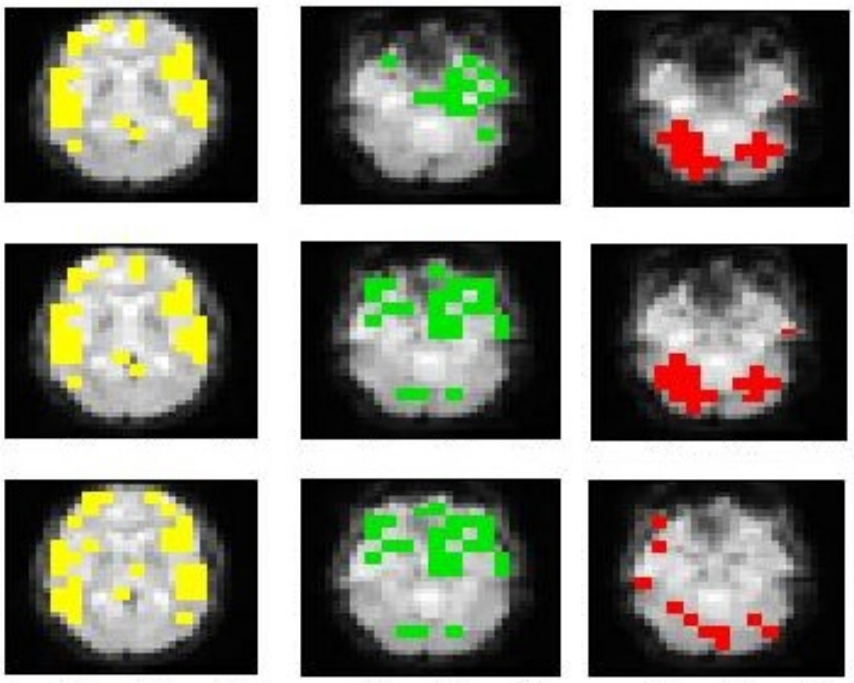

(a) (b) (c)

Figure 4.3: Optimal *EigenBrains* network architecture for *Language* $threshold_1$ and $threshold_2 = 9$ and $threshold_3 = 6$. (a) EigenBrain 2 - slices 13/14/15 (b) EigenBrain 4 - slices 8/9/10 (c) EigenBrain 5 - slices 7/8/9. Slices are numbered from the top to the bottom

4.3 Prediction performance

Fig 4.7 shows the prediction scores for several values of sparsity for the features *Body Parts*, *Faces*, *Language*, and *Body Parts*; for $m = 14$.

We show in Fig 4.5 that the first *Eigenbrain* selects almost all the voxels in the brain so it can be considered total brain activation. To study how *Eigenbrain 1* (e_1) affects to prediction (see Fig. 4.8 and see Fig. 4.9) we project X into the regular subspace E_{brain} and onto E^1_{brain}. In some cases it performs better without projecting onto e_1.

$$E^1_{brain} = \begin{bmatrix} e_2(1) & \cdots & e_m(1) \\ \vdots & \vdots & \vdots \\ e_2(p) & \cdots & e_m(p) \end{bmatrix}$$

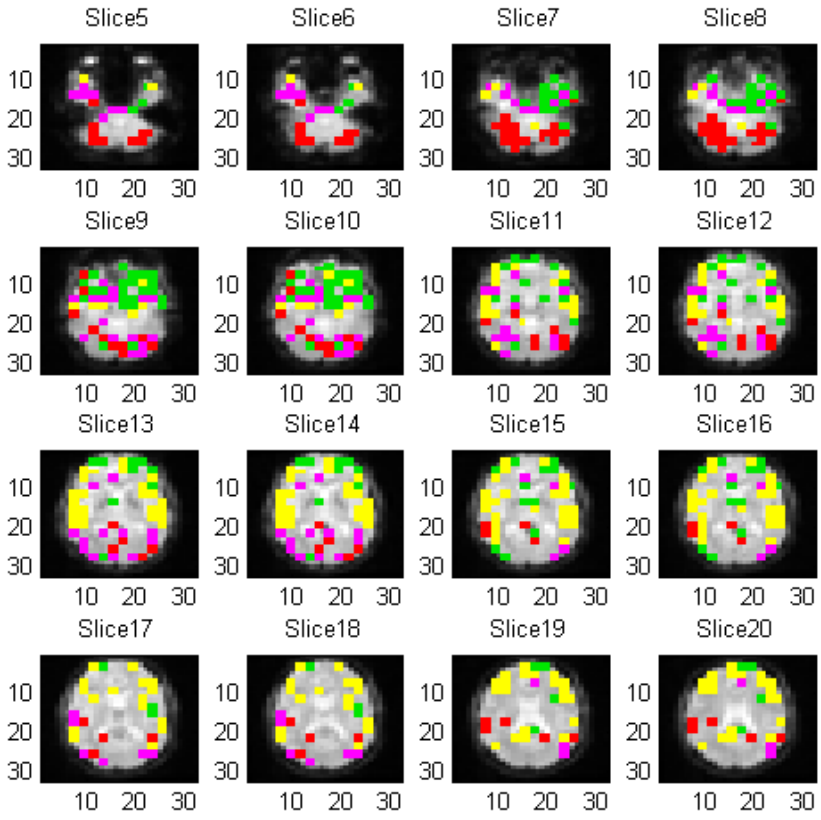

Figure 4.4: Overlap of e_2 (yellow), e_3 (pink), e_4 (green) and e_5 (red) for subspace $m = 14$

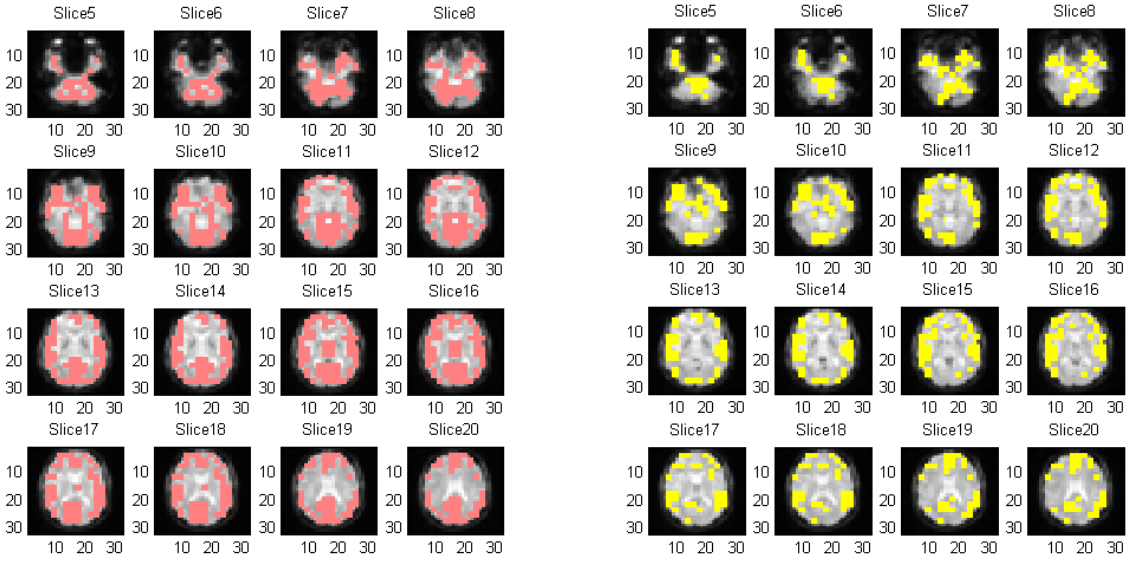

(a)

(b)

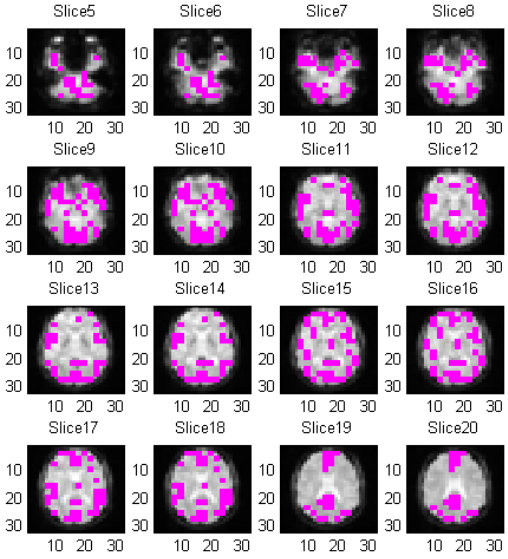

(c)

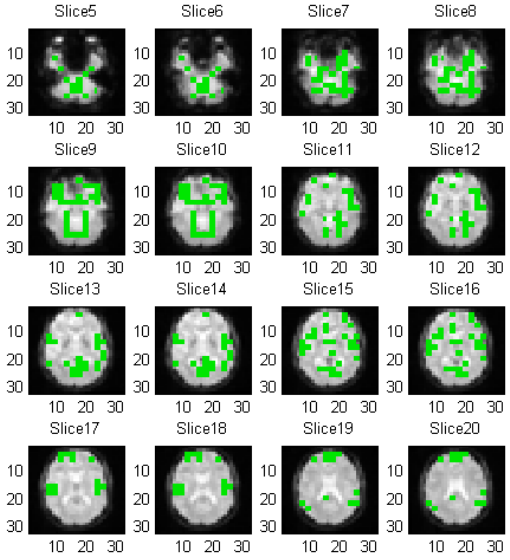

(d)

Figure 4.5: Optimal *EigenBrains* network architecture for *Faces* $threshold_1$ and $threshold_2 = 3$ and $threshold_3 = 2$. (a) EigenBrain 1 (b) EigenBrain 2 (c) EigenBrain 3 (d) EigenBrain 4

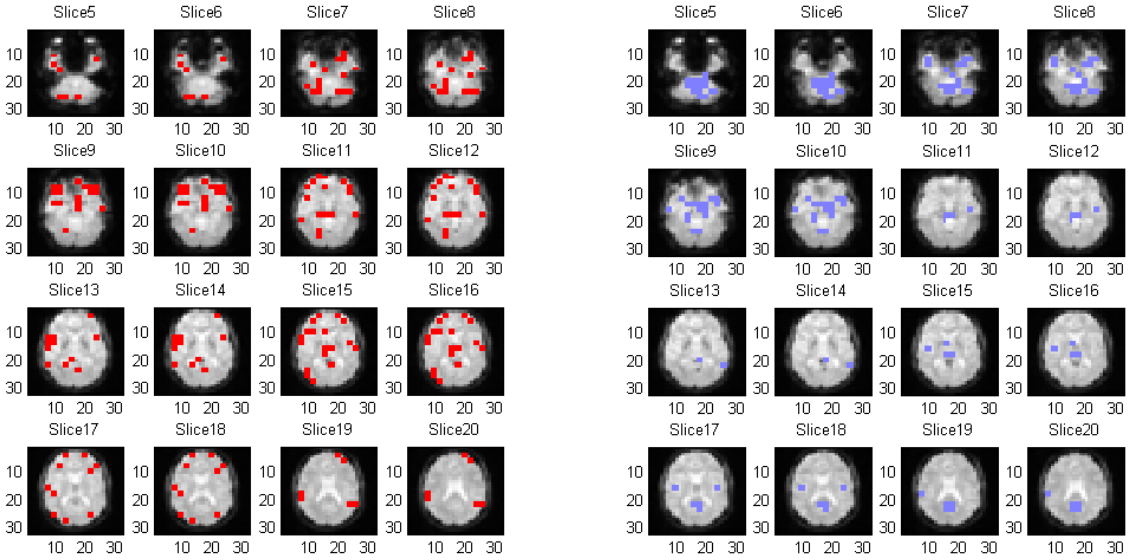

(a) (b)

Figure 4.6: Optimal *EigenBrains* network architecture for *Faces* $threshold_1$ and $threshold_2 = 3$ and $threshold_3 = 2$.(e) EigenBrain 5 (f) EigenBrain 6

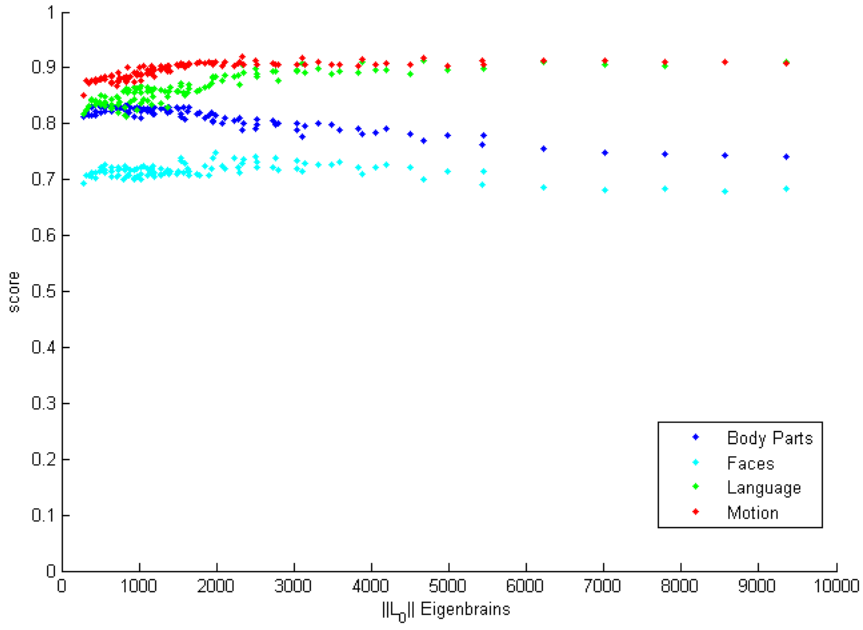

Figure 4.7: Kernel Ridge Regression Prediction score for $m = 14$

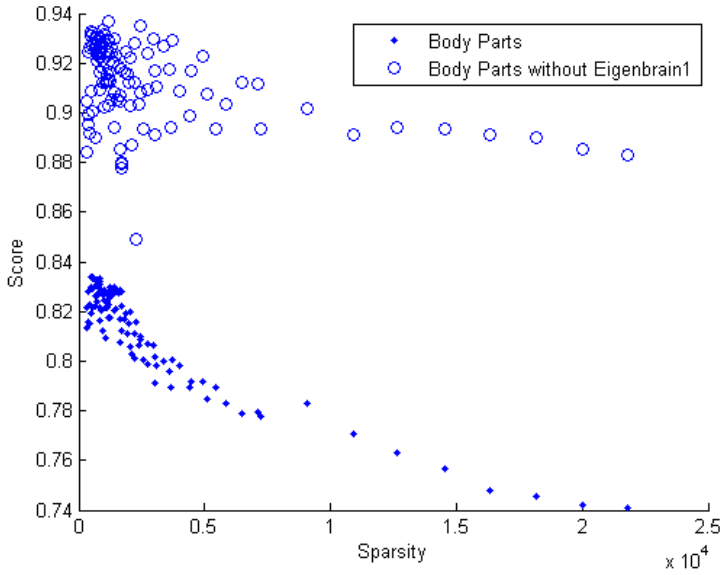

(a)

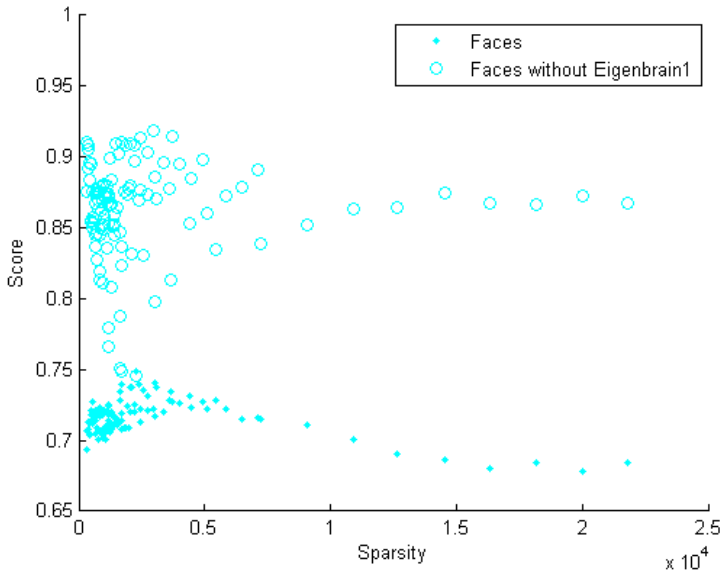

(b)

Figure 4.8: Prediction scores vs Sparsity for subspaces E_{brain} and E^1_{brain} . (a) Body Parts (b) Faces

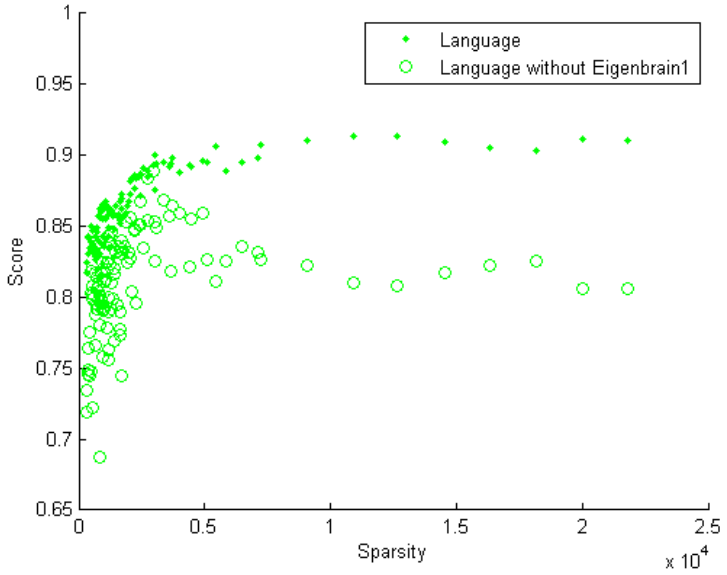

(a)

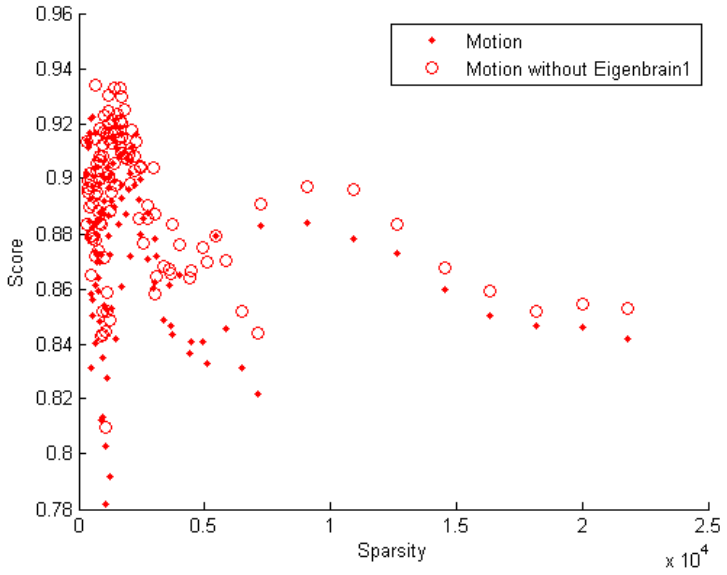

(b)

Figure 4.9: Prediction scores vs Sparsity for subspaces E_{brain} and E^1_{brain} . (c) Language (d) Motion

Chapter 5

Discussion and conclusion

In this thesis, we propose a new method for the analysis of fMRI data. Our approach discovers clustered brain areas by using sparse PCA representations without any spatial constraint in the optimization problem. We do not apply any spatial smoothing function in addition to the sparse coordinate selection, however, the principal components appear to be concentrated around specific areas in the cerebral cortex, which are really helpful in the interpretation stage.

We have proposed a technique to identify a low dimensional neuronal network subspace E_{brain} , where all the principal components are p-dimensional vectors ($\in \mathbb{R}^p$), also called *Eigenbrains*. Only some few entries from each of them are different than 0, and the sparsity is controlled by λ_1, λ_2 and λ_3. We allow the E_{brain} to be different for each task developed in the brain. Within an specific subspace, the sparsity increases according to the index of the *Eigenbrain*($\|e_1\|_0 > \|e_2\|_0$).

The adaptive combination of *Eigenbrains* defines the brain activation for a specific feature. The combination of *Eigenbrains* can be interpreted according to the massive modularity hypothesis. Each *Eigenbrain* can be understood as a small number of well defined functional areas (some of them coincide with Brodmann areas).

It is worth noticing the efficiency of this semi-supervised method. With a small number ($m = 14$) of extremely sparse *Eigenbrains* and relative sparsity values in the range from 0.72% to 0.12% we achieve final prediction scores ranging from 0.7 to 0.92 for the studied features. This implies a really small computation time cost. The approach performs competitively in terms of prediction score compared with other submissions to the PBAIC contest. As a general rule, the

more components we include in the new low-dimensional subspace, the more variance is captured and the better the performance is in terms of prediction, nevertheless, there exists the special behavior of the first *Eigenbrain*.

The model obtained with this approach is interpretable because the input fMRI data is very rich in external stimulus. On the other hand, the features corresponding with expected diffuse brain activation, such as self-awareness, might not be well predicted.

Bibliography

[1] T. Hastie, R. Tibshirani, and J. Friendman, The Elements of Statistical Learning: Data Mining, Inference, and Prediction. Springer, Second Edition.

[2] F. Meyer and X. Shen, "Classification of fmri time series in a low-dimensional subspace with a spatial prior," Medical Imaging, IEEE Transactions on, vol. 27, no. 1, pp. 87 –98, jan. 2008.

[3] S. Achard and E. Bullmore, "Efficiency and cost of economical brain functional networks," PLoS Computational Biology, vol. 3, no. 2, 2007.

[4] [Online]. Available: http://pbc.lrdc.pitt.edu

[5] [Online]. Available: http://www.brainvoyager.com/

[6] M. K. Carroll, G. A. Cecchi, I. Rish, R. Garg, and A. R. Rao, "Prediction and interpretation of distributed neural activity with sparse models," NeuroImage, vol. 44, no. 1, pp. 112 – 122, 2009. [Online]. Available: http://www.sciencedirect.com/science/article/pii/S1053811908009415

[7] G. Valente, F. D. Martino, F. Esposito, R. Goebel, and E. Formisano, "Predicting subject-driven actions and sensory experience in a virtual world with relevance vector machine regression of fmri data." NeuroImage, vol. 56, no. 2, pp. 651–661, 2011.

[8] A. Woolgar, R. Thompson, D. Bor, and J. Duncan, "Multi-voxel coding of stimuli, rules, and responses in human frontoparietal cortex," NeuroImage, vol. 56, no. 2, pp. 744 – 752, 2011, ¡ce:title¿Multivariate Decoding and Brain Reading¡/ce:title¿. [Online]. Available: http://www.sciencedirect.com/science/article/pii/S1053811910004477

[9] J. Ylipaavalniemi, E. Savia, S. Malinen, R. Hari, R. Vigrio, and S. Kaski, "Dependencies between stimuli and spatially independent fmri sources: Towards brain correlates of natural stimuli," NeuroImage, vol. 48, no. 1, pp. 176 – 185, 2009.

[10] A. Battle, G. Chechik, and D. Koller, "Temporal and cross-subject probabilistic models for fmri prediction tasks," in Advances in Neural Information Processing Systems 19, B. Schölkopf, J. Platt, and T. Hoffman, Eds. Cambridge, MA: MIT Press, 2007, pp. 121–128.

[11] E. Olivetti, D. Sona, and S. Veeramachaneni, "Gaussian process regression and recurrent neural networks for fmri image classification," ICT International Doctorate School, university of trento, Tech. Rep., 2006, pBAIC.

[12] G. Yourganov, X. Chen, A. S. Lukic, C. L. Grady, S. L. Small, M. N. Wernick, and S. C. Strother, "Dimensionality estimation for optimal detection of functional networks in bold fmri data." NeuroImage, no. 2, pp. 531–543.

[13] R. Samuels, "Evolutionary psychology and the massive modularity hypothesis," vol. 49, no. 4, pp. 575–602, 1998.

[14] D. Buller, "Get over: Massive modularity," Biology and Philosophy, vol. 20, pp. 881–891, 2005. [Online]. Available: http://dx.doi.org/10.1007/s10539-004-1602-3

[15] D. Paul and I. M. Johnstone, "Augmented sparse principal component analysis for high dimensional data," arXiv.org 1202.1242v1[math.ST], 2012.

[16] B. Moghaddam, Y. Weiss, and S. Avidan, "Spectral bounds for sparse pca: Exact and greedy algorithms," in Advances in Neural Information Processing Systems. MIT Press, 2006, pp. 915–922.

[17] Z. Ma, "Sparse principal component analysis and iterative thresholding," arXiv.org 1112.2432v1[math.ST], 2011.

[18] B. Nadler, "Discussion of on consistency and sparsity for principal component analysis in high dimensions by johnstone and lu," J. Am. Stat. Assoc., 2009.

[19] H. Shen and J. Z. Huang, "Sparse principal component analysis via regularized low rank matrix approximation," Journal of Multivariate Analysis, vol. 99, no. 6, pp. 1015 – 1034, 2008. [Online]. Available: http://www.sciencedirect.com/science/article/pii/S0047259X07000887

[20] M. Journée, Y. Nesterov, P. Richtárik, and R. Sepulchre, "Generalized power method for sparse principal component analysis," J. Mach. Learn. Res., vol. 11, pp. 517–553, Mar. 2010. [Online]. Available: http://dl.acm.org/citation.cfm?id=1756006.1756021

[21] M. Johnstone, "On the distribution of the largest eigenvalue in principal components analysis," Ann. Statist, vol. 29, pp. 295–327, 2001.

[22] I. M. Johnstone and A. Y. Lu, "Sparse Principal Components Analysis," ArXiv e-prints, Jan. 2009.

[23] J. Bickel and E. Levina, "Covariance regularization by thresholding," Tech. Rep., 2007.

[24] V. D. Calhoun, T. Adali, L. K. Hansen, J. Larsen, and J. J. Pekar, "Ica of functional mri data: An overview," in in Proceedings of the International Workshop on Independent Component Analysis and Blind Signal Separation, 2003, pp. 281–288.

[25] C.-C. Chen, C. W. Tyler, and H. A. Baseler, "Statistical properties of bold magnetic resonance activity in the human brain," NeuroImage, vol. 20, no. 2, pp. 1096 – 1109, 2003. [Online]. Available: http://www.sciencedirect.com/science/article/pii/S1053811903003586

[26] E. Bullmore, C. Long, J. Suckling, J. Fadili, G. Calvert, F. Zelaya, T. A. Carpenter, and M. Brammer, "Colored noise and computational inference in neurophysiological (fmri) time series analysis: Resampling methods in time and wavelet domains," Human Brain Mapping, vol. 12, no. 2, pp. 61–78, 2001. [Online]. Available: http://dx.doi.org/10.1002/1097-0193(200102)12:2¡61::AID-HBM1004¿3.0.CO;2-W

[27] F. Meyer and G. Stephens, "Locality and low-dimensions in the prediction of natural experience from fmri," in Advances in Neural Information Processing Systems 20, J. Platt, D. Koller, Y. Singer, and S. Roweis, Eds. Cambridge, MA: MIT Press, 2008, pp. 1001–1008.

[28] [Online]. Available: http://www.fil.ion.ucl.ac.uk/spm/software/spm8/

[29] H. Zou, T. Hastie, and R. Tibshirani, "Sparse principal component analysis," Journal of Computational and Graphical Statistics, vol. 15, no. 2, pp. 265–286, 2006. [Online]. Available: http://www.tandfonline.com/doi/abs/10.1198/106186006X113430

[30] N. Hurley and S. Rickard, "Comparing measures of sparsity," Information Theory, IEEE Transactions on, vol. 55, no. 10, pp. 4723 –4741, oct. 2009.

[31] E. Bullmore and O. Sporns, "Complex brain networks: graph theoretical analysis of structural and functional systems," NATURE REVIEWS NEUROSCIENCE, vol. 10, no. 3, pp. 186–198, MAR 2009.